

# AFFSegNet: Adaptive Feature Fusion Segmentation Network for Microtumors and Multi-Organ Segmentation

Fuchen Zheng<sup>1,2</sup>, Xinyi Chen<sup>3</sup>, Xuhang Chen<sup>1,2</sup>, Haolun Li<sup>1</sup>, Xiaojiao Guo<sup>1</sup>, Guoheng Huang<sup>4</sup>, Chi-Man Pun<sup>1\*</sup>, and Shoujun Zhou<sup>2\*</sup>

<sup>1</sup>University of Macau

<sup>2</sup>Shenzhen Institute of Advanced Technology, Chinese Academy of Sciences

<sup>3</sup>Southern University of Science and Technology

<sup>4</sup>Guangdong University of Technology

**Abstract**—Medical image segmentation, a crucial task in computer vision, facilitates the automated delineation of anatomical structures and pathologies, supporting clinicians in diagnosis, treatment planning, and disease monitoring. Notably, transformers employing shifted window-based self-attention have demonstrated exceptional performance. However, their reliance on local window attention limits the fusion of local and global contextual information, crucial for segmenting microtumors and miniature organs. To address this limitation, we propose the Adaptive Feature Fusion Segmentation Network (AFFSegNet), a transformer architecture that effectively integrates local and global features for precise medical image segmentation. AFFSegNet comprises a transformer-based U-shaped encoder-decoder network. The encoder utilizes shifted window self-attention across five resolutions to extract multi-scale features, which are then propagated to the decoder through skip connections. We introduce an augmented multi-layer perceptron within the encoder to explicitly model long-range dependencies during feature extraction. Recognizing the constraints of conventional symmetrical encoder-decoder designs, we propose an Adaptive Feature Fusion (AFF) decoder to complement our encoder. This decoder incorporates three key components: the Long Range Dependencies (LRD) block, the Multi-Scale Feature Fusion (MFF) block, and the Adaptive Semantic Center (ASC) block. These components synergistically facilitate the effective fusion of multi-scale features extracted by the decoder while capturing long-range dependencies and refining object boundaries. Comprehensive experiments on diverse medical image segmentation tasks, including multi-organ, liver tumor, and bladder tumor segmentation, demonstrate that AFFSegNet achieves state-of-the-art results. Code and models are available at: <https://github.com/lzeeorno/AFFSegNet>.

**Index Terms**—Medical Image Segmentation, Vision Transformer, Attention Mechanism, Multi-scale Feature Fusion

## I. INTRODUCTION

Current research in medical image segmentation focuses on critical tasks such as tumor segmentation and organ delineation. Consequently, neural network architectures from the broader field of computer vision are being increasingly adapted for medical image analysis. Vision transformers [1] have gained significant traction due to their robust feature extraction capabilities. However, while advancements in multi-head self-attention attention within these transformers have yielded impressive results, challenges remain. These models often struggle to capture features of small objects due to limitations in combine the modeling long-range dependencies [2] and accurately delineating image edges. Consequently, effectively integrating multi-scale local and global features remains an ongoing challenge. To address these limitations, we propose the Adaptive Feature Fusion Segmentation Network (AFFSegNet), a novel hybrid CNN [3]-Transformer [1]-based architecture specifically designed for image segmentation. Inspired by the strengths of Swin-transformer [4], AFFSegNet leverages Transformer blocks within a U-shaped residual

structure to enhance feature learning across multiple scales. Furthermore, recognizing the limitations of simply replicating encoder structures in the decoder, we introduce a novel Adaptive Feature Fusion (AFF) decoder. This decoder comprises three key components: the Long Range Dependencies (LRD) block, the Multi-Scale Feature Fusion (MFF) block, and the Adaptive Semantic Center (ASC) block. These components work synergistically to leverage encoder-derived features effectively, enabling the accurate segmentation of small structures, particularly at edges, and facilitating robust multi-scale feature fusion. AFFSegNet achieves state-of-the-art performance on various medical image segmentation tasks. Notably, AFFSegNet surpasses previous state-of-the-art models, demonstrating impressive improvements on the LiTS2017, ISICDM2019 and Synapse datasets, respectively. The main contributions of this paper are as follows:

- 1) We introduce **AFFSegNet**, a hybrid model that combines the strengths of ResUnet and Swin-transformer, incorporating window attention, spatial attention, U-shaped architecture, and residual connections for efficient segmentation.
- 2) We propose an **Adaptive Feature Fusion (AFF) Decoder** that maximizes the synergistic potential of window attention to capture multi-scale local and global information by fusing feature maps of varying scales.
- 3) Extensive experiments demonstrate that the proposed AFFSegNet achieves new state-of-the-art results on various medical image segmentation datasets.

## II. METHODOLOGY

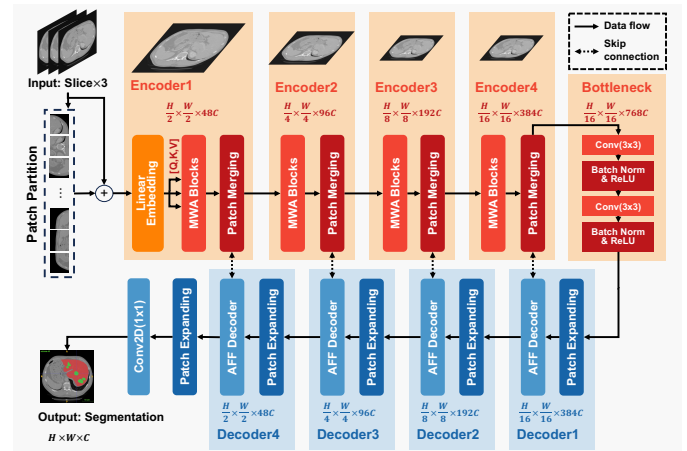


Fig. 1. Overview of the ASSNet architecture.

\* Corresponding authors.

### A. MWA Transformer Block

The MWA Transformer block forms the backbone of AFFSegNet. As shown in Figure 2, it substitutes the Multi-Head Self-Attention (MSA) module [5] in the standard Transformer layer with a shifted window attention-based MSA module, while preserving other attention-related components. Each MWA block consists of a shifted window-based MSA module followed by an Enhanced Feed-Forward Network (EFFN).

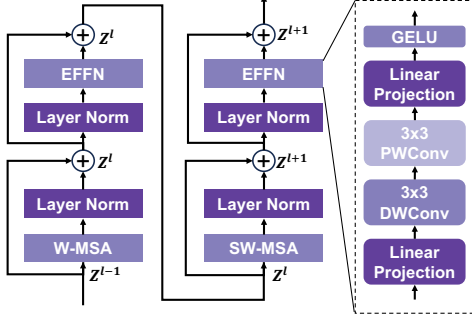


Fig. 2. This figure presents details of a schematic diagram of the proposed Multi-scale Window Attention (MWA) transformer block.

Recognizing the limitations of standard FFNs in capturing local context [6], [7], we enhance the MLP within our Transformer block by incorporating depth-wise and pixel-wise convolutions [8]–[10]. As depicted in Figure 2, the EFFN first projects input tokens to a higher dimensional space. The projected tokens are then reshaped into 2D feature maps and processed by a  $3 \times 3$  pixel-wise convolution followed by a  $3 \times 3$  depth-wise convolution, effectively capturing local contextual information. Subsequently, the features are reshaped back into tokens and projected back to the original channel dimension. Finally, a GELU activation function [11] introduces non-linearity.

Mathematically, the computation within an MWA transformer block can be expressed as:

$$\begin{aligned} \hat{X}^l &= \text{W-MSA}(\text{LN}(X^{l-1})) + X^{l-1}, \\ X^l &= \text{EFFN}(\text{LN}(\hat{X}^l)) + \hat{X}^l, \\ \hat{X}^{l+1} &= \text{SW-MSA}(\text{LN}(X^l)) + X^l, \\ X^{l+1} &= \text{EFFN}(\text{LN}(\hat{X}^{l+1})) + \hat{X}^{l+1}, \end{aligned} \quad (1)$$

where  $\hat{X}^l$  and  $\hat{X}^{l+1}$  represent the output from window-based multi-head self-attention using regular (W-MSA) and shifted window partitioning configurations (SW-MSA), respectively; LN and EFFN denote layer normalization and the proposed enhanced feed-forward network illustrated in Figure 2, respectively.

Following previous work [12], [13], we incorporate a relative position bias  $B$  within the self-attention computation to enhance performance. The attention calculation is formulated as:

$$\text{Attention}(Q, K, V) = \text{SoftMax} \left( \frac{QK^T}{\sqrt{d}} + B \right) V, \quad (2)$$

where  $B$  is derived from a smaller parameterized bias matrix  $\hat{B} \in \mathbb{R}^{(2M-1) \times (2M-1)}$ ;  $Q$ ,  $K$ , and  $V$  represent the query, key, and value matrices, respectively; and  $d$  is the dimension of the query and key features.

### B. Adaptive Feature Fusion (AFF) Decoder

To address the limitations of vision transformers in capturing local information [2], [12] and the inadequacies of existing decoders

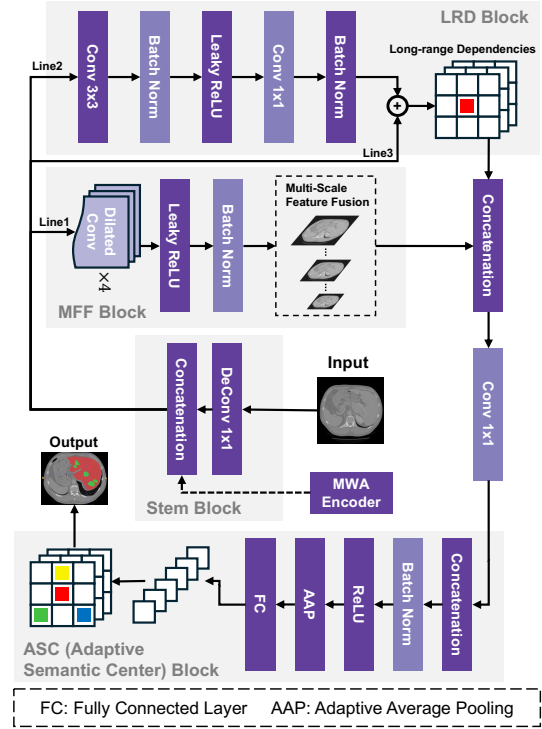


Fig. 3. This figure presents details of a schematic diagram of the proposed Adaptive Feature Fusion (AFF) Decoder.

in integrating multi-scale local and global features [13]–[15], we propose an Adaptive Feature Fusion (AFF) Decoder. The AFF decoder comprises Long-Range Dependencies (LRD) block, Multi-scale Feature Fusion (MFF) block, and Adaptive Semantic Center (ASC) block, as illustrated in Figure 3. The AFF decoder begins with a standard deconvolution operation to restore the feature map to the original image size while preserving resolution. This enriched feature map then undergoes three parallel operations. First, spatial attention using dilated convolutions with dilation rates of 1, 6, 12, and 18 is applied to capture multi-scale details [16]. LeakyReLU [17] is utilized as the activation function in the decoder to mitigate the vanishing gradient problem and enhance model stability and generalization. Second, an LRD block, implemented using a series of convolutions and LeakyReLU activations, models long-range dependencies. Finally, a third parallel thread acts as a mask prompt, aiding the decoding process of the first two threads. The resulting feature map is then passed to the ASC block. Drawing inspiration from the Sobel edge detection method [18], the ASC block extracts local region information and performs channel-wise enhancement. It achieves this by utilizing an enhanced filter generated from adaptive average pooling [19] and a fully connected layer [20].

### C. Objective Function

During training, AFFSegNet employs the BCE Dice loss  $\mathcal{L}_{BD}$  [29], a combination of Binary Cross-Entropy (BCE) loss  $\mathcal{L}_{BCE}$  and Dice loss  $\mathcal{L}_D$ , widely used in medical image segmentation tasks. This loss function is defined as:

$$\mathcal{L}_{BD} = \frac{1}{N} \sum_{i=1}^N \left( 1 - \frac{2 \sum_j y_{i,j} p_{i,j}}{\sum_j y_{i,j} + \sum_j p_{i,j}} \right) - (y \log(p) + (1-y) \log(1-p)), \quad (3)$$

where  $y$  represents the ground truth segmentation mask,  $p$  denotes the predicted segmentation mask, and  $N$  is the number of pixels

TABLE I  
COMPARISON WITH STATE-OF-THE-ART MODELS ON THE ISICDM2019 AND LITS2017 DATASETS. THE BEST RESULTS ARE BOLDIED WHILE THE SECOND BEST ARE UNDERLINED.

Model	ISIDM2019				LITS2017			
	Average		Bladder	Tumor	Average		Liver	Tumor
	DSC(%) $\uparrow$	mIoU(%) $\uparrow$	DSC(%) $\uparrow$	DSC(%) $\uparrow$	DSC(%) $\uparrow$	mIoU(%) $\uparrow$	DSC(%) $\uparrow$	DSC(%) $\uparrow$
R50-ViT [1]+CUP [21]	88.77	85.62	92.05	85.49	82.62	79.68	85.83	79.41
TransUNet [21]	<u>94.56</u>	<u>93.60</u>	<u>97.74</u>	<u>91.38</u>	<u>93.29</u>	<u>90.81</u>	<u>95.54</u>	<u>91.03</u>
SwinUNet [15]	91.95	89.77	94.73	89.17	89.68	86.62	93.31	86.04
Swin UNETR [13]	92.60	90.61	95.08	90.12	91.95	90.02	94.73	89.17
UNETR [22]	91.55	88.34	94.83	88.26	89.38	87.46	92.89	85.86
nnFormer [23]	93.69	89.11	96.97	90.41	91.74	89.95	94.57	88.91
SAM [24]+Manual Prompt	34.16	23.4	59.10	9.22	27.33	17.21	46.10	8.56
MedSAM [25]	53.17	37.16	65.3	41.03	73.36	60.73	90.1	56.61
<b>ASSNet (Ours)</b>	<b>96.75</b>	<b>96.04</b>	<b>98.87</b>	<b>94.63</b>	<b>95.47</b>	<b>94.88</b>	<b>96.79</b>	<b>94.14</b>

TABLE II  
COMPARISON WITH STATE-OF-THE-ART MODELS ON THE SYNAPSE MULTI-ORGAN DATASET. THE BEST RESULTS ARE BOLDIED WHILE THE SECOND BEST ARE UNDERLINED.

Model	Average DSC(%) $\uparrow$	Aotra DSC(%) $\uparrow$	Gallbladder DSC(%) $\uparrow$	Kidney(Left) DSC(%) $\uparrow$	Kidney(Right) DSC(%) $\uparrow$	Liver DSC(%) $\uparrow$	Pancreas DSC(%) $\uparrow$	Spleen DSC(%) $\uparrow$	Stomach DSC(%) $\uparrow$
R50-ViT [1]+CUP [21]	71.29	73.73	55.13	75.80	72.20	91.51	45.99	81.99	73.95
TransUNet [21]	84.37	90.68	71.99	86.04	83.71	95.54	73.96	88.80	84.20
SwinUNet [15]	79.13	85.47	66.53	83.28	79.61	94.29	56.58	90.66	76.60
UNETR [22]	79.57	89.99	60.56	85.66	84.80	94.46	59.25	87.81	73.99
Swin UNETR [13]	83.51	<u>90.75</u>	66.72	86.51	85.88	95.33	70.07	<b>94.59</b>	78.20
CoTr [26]	80.74	85.42	68.93	85.45	83.62	93.89	63.77	88.58	76.23
nnFormer [23]	85.32	90.72	71.67	85.60	87.02	<u>96.28</u>	82.28	87.30	81.69
SAM [24]+Manual Prompt	58.55	61.20	54.30	79.10	68.60	46.10	51.10	51.80	56.20
MedSAM [25]	82.55	87.20	76.60	88.50	81.40	90.10	76.00	75.10	85.50
SAM 2 [27]	53.39	40.00	77.20	64.20	72.40	27.00	68.20	36.60	41.50
MedSAM-2 [28]	<u>89.08</u>	89.40	<b>92.70</b>	92.10	92.40	83.60	<b>83.20</b>	91.80	<u>87.40</u>
<b>ASSNet (Ours)</b>	<b>90.73</b>	<b>93.02</b>	<u>87.08</u>	<b>92.67</b>	<b>93.06</b>	<b>97.11</b>	<u>82.97</u>	<u>92.19</u>	<b>87.72</b>

in the image. This combination effectively enhances both pixel-wise classification accuracy and boundary delineation.

### III. EXPERIMENTS

In this section, we present the experimental framework and discuss the results. First, we describe the datasets and evaluation metrics employed. Next, we compare the performance of AFFSegNet against state-of-the-art methods in medical image segmentation. Finally, we conduct ablation studies to investigate the impact of individual components in the AFFSegNet architecture.

#### A. Implementation Details

In all experiments, we adhered to the training, validation, and test splits provided by nnformer [23] to ensure consistency and facilitate fair comparisons with other methods. This resulted in splits of 80%, 15%, and 5% for training, validation, and testing, respectively. All input images were resized to a resolution of  $512 \times 512$  pixels. The Stochastic Gradient Descent (SGD) [30] optimizer was employed with a momentum of 0.98 and a weight decay of  $1 \times 10^{-6}$ . The learning rate was subsequently decreased using a cosine decay strategy to a minimum of  $6 \times 10^{-6}$ . Data augmentation during training included random horizontal flipping and rotation. Some comparison results are referenced from nnformer [23], SAM [31], [32], and MedSAM2 [28].

We assessed the segmentation performance using two widely recognized metrics:

1) *Dice Coefficient Score* [33]: The Dice Similarity Coefficient (DSC) quantifies the overlap between the predicted segmentation and the ground truth.

2) *Mean Intersection over Union (mIoU)*: The mean Intersection over Union (mIoU) calculates the average ratio of intersection to union between the predicted segmentation and the ground truth across all classes.

#### B. Comparisons with State-of-the-Art Methods

We compared the performance of AFFSegNet with several state-of-the-art medical image segmentation methods on the three datasets described above. The results are summarized in Tables I and II.

1) *Liver Tumor Segmentation*: Table I presents the results on the LiTS2017 [34] dataset. AFFSegNet outperforms all other methods, achieving an average DSC of 95.47% and an mIoU of 94.88%. Notably, AFFSegNet surpasses the second-best model, TransUNet [21], by a significant margin (DSC: +2.19%, mIoU: +4.07%). This improvement highlights AFFSegNet’s ability to accurately segment small and irregularly shaped tumors, which can be attributed to the Multi-Scale Feature Fusion (MFF) block within the AFF Decoder. The MFF block effectively captures features across multiple scales, enabling the network to delineate fine-grained tumor boundaries. Interestingly, the popular segmentation models SAM [24], [31] and MedSAM [25] struggle to accurately segment multiple tumors with varying shapes and sizes within a single image even they pretrained on large datasets. This suggests that AFFSegNet’s architectural advantages provide it with an edge in handling such complex segmentation scenarios.

2) *Bladder Tumor Segmentation*: On the ISICDM2019 [35] dataset, AFFSegNet again demonstrates superior performance, achieving an average DSC of 96.75% and an mIoU of 96.04% as shown in Table I. This represents a substantial improvement of 3.25% in DSC compared to the second-best method. The remarkable

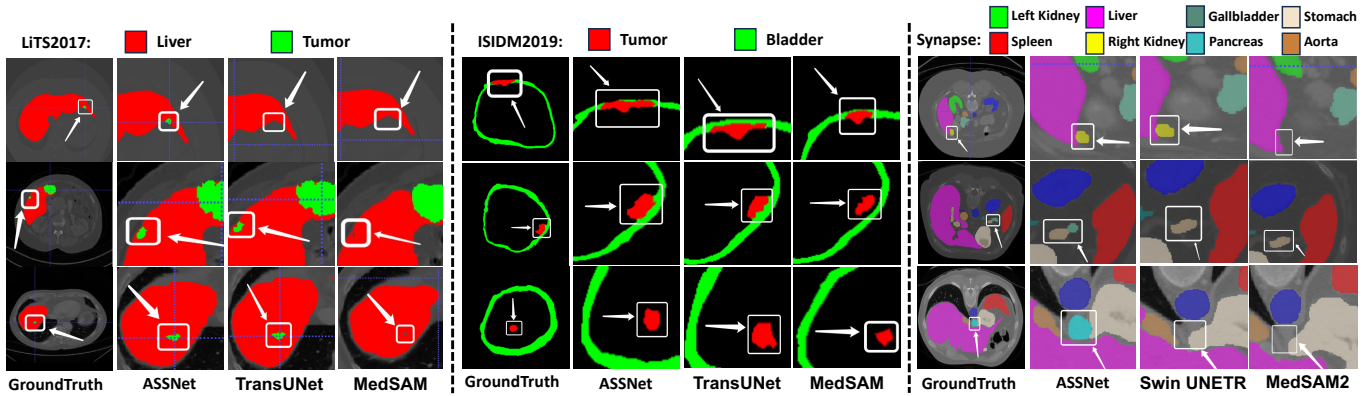


Fig. 4. LiTS2017, ISICDM2019 and Synapse Prediction Results

performance on bladder tumor segmentation can be attributed to the ASC block in the AFF decoder, which effectively captures local region information critical for accurate boundary delineation. These results underscore the robustness and adaptability of AFFSegNet across different tumor types and imaging modalities.

3) *Multi-Organ Segmentation*: The results for the Synapse [36] multi-organ segmentation dataset are presented in Table II. AFFSegNet achieves state-of-the-art results with an average DSC of 90.73% and AFFSegNet consistently achieves high scores across all organs, demonstrating its ability to generalize to different anatomical structures. Notably, AFFSegNet excels in segmenting smaller organs, achieving the highest DSC scores for five out of the eight organs. This robust performance on a challenging multi-organ dataset highlights the effectiveness of AFFSegNet’s U-shaped architecture and AFF decoder in preserving both high-level semantic information and low-level spatial details.

#### IV. VISUALIZATION OF SEGMENTATION RESULTS

To visually assess the segmentation capabilities of AFFSegNet, Figure 4 presents qualitative comparisons against other state-of-the-art methods on representative slices from the LiTS2017, ISICDM2019, and Synapse datasets. AFFSegNet accurately segments small tumor nodules on the liver periphery and preserves the integrity of miniature organs, which are often missed or inaccurately segmented by other methods. These visual comparisons further emphasize the accuracy and robustness of AFFSegNet in challenging medical image segmentation scenarios.

#### V. ABLATION STUDY

TABLE III  
ABLATION STUDY OF DIFFERENT MODULES IN ASSNET.

EFFN	LRD	MFF	ASC	ISICDM2019	LiTS2017
×	✓	✓	✓	93.91%	92.56%
✓	×	✓	✓	75.54%	73.92%
✓	✓	×	✓	87.15%	85.10%
✓	✓	✓	×	88.93%	87.22%
✓	✓	✓	✓	96.75%	95.47%

To investigate the contribution of each module within AFFSegNet, we conducted an ablation study on the ISICDM2019 and LiTS2017 datasets. We used the same experimental setup as described in Section III-A and evaluated the performance of AFFSegNet by

removing one component at a time. The results, summarized in Table III, demonstrate that all components contribute to the overall performance of AFFSegNet.

The ablation study clearly shows that the Embedded Feature Fusion Network (EFFN) significantly enhances AFFSegNet’s ability to model long-range dependencies. Removing EFFN leads to a considerable drop in performance. This highlights the importance of EFFN in capturing long-range interactions between image regions. Similarly, the LRD block in the AFF decoder plays a crucial role in preserving long-range dependencies and establishing a connection between the encoder and decoder. Removing the LRD block results in a substantial decline in performance, with average DSCs dropping to 75.54% and 73.92% for the two datasets, respectively. This confirms the essential function of the LRD block. The MFF and ASC blocks within the decoder also contribute significantly to AFFSegNet’s state-of-the-art performance. Removing the MFF block leads to a decrease in average DSC to 87.15% and 85.10% for the two datasets, respectively, demonstrating the importance of multi-scale feature fusion in medical image segmentation. The ASC block, on the other hand, focuses on detecting critical edges and central features, which are essential for accurate boundary delineation.

#### VI. CONCLUSION

The hallmark of AFFSegNet lies in its innovatively and effectively integrating an EFFN, a LRD block, a MFF block, and an ASC block, so that it exhibits superior capacity in modeling long-range dependencies and capturing salient features across varying scales and spatial contexts. Rigorous evaluation on three publicly available medical image segmentation datasets demonstrated that AFFSegNet consistently achieves state-of-the-art segmentation performance, surpassing existing methods in accurately delineating diverse anatomical structures and pathologies. These promising results highlight AFFSegNet’s potential as a robust and valuable tool for assisting medical professionals in critical tasks such as diagnosis, treatment planning, and disease monitoring. Future research will investigate the generalizability of AFFSegNet to other medical imaging modalities and further evaluate its performance in more complex clinical scenarios.

#### ACKNOWLEDGMENT

This work was supported in part by the National Key R&D Project of China (2018YFA0704102, 2018YFA0704104), in part by Natural Science Foundation of Guangdong Province (No. 2023A1515010673), and in part by Shenzhen Technology Innovation

Commission (No. JSGG20220831110400001), in part by Shenzhen Development and Reform Commission (No. XMHT20220104009).

## REFERENCES

- [1] A. Dosovitskiy, L. Beyer, A. Kolesnikov, D. Weissenborn, X. Zhai, T. Unterthiner, M. Dehghani, M. Minderer, G. Heigold, S. Gelly, J. Uszkoreit, and N. Houlsby, "An image is worth 16x16 words: Transformers for image recognition at scale," in *International Conference on Learning Representations*, 2021.
- [2] S. Wang, L. Zhou, Z. Gan, Y.-C. Chen, Y. Fang, S. Sun, Y. Cheng, and J. Liu, "Cluster-former: Clustering-based sparse transformer for long-range dependency encoding," *arXiv*, 2020.
- [3] Y. LeCun, L. Bottou, Y. Bengio, and P. Haffner, "Gradient-based learning applied to document recognition," *Proceedings of the IEEE*, vol. 86, no. 11, pp. 2278–2324, 1998.
- [4] Z. Liu, Y. Lin, Y. Cao, H. Hu, Y. Wei, Z. Zhang, S. Lin, and B. Guo, "Swin transformer: Hierarchical vision transformer using shifted windows," in *Proceedings of the IEEE/CVF international conference on computer vision*, 2021, pp. 9992–10002.
- [5] A. Vaswani, N. Shazeer, N. Parmar, J. Uszkoreit, L. Jones, A. N. Gomez, L. Kaiser, and I. Polosukhin, "Attention is all you need," in *Advances in Neural Information Processing Systems*, 2017, pp. 5998–6008.
- [6] H. Wu, B. Xiao, N. Codella, M. Liu, X. Dai, L. Yuan, and L. Zhang, "Cvt: Introducing convolutions to vision transformers," in *Proceedings of the IEEE/CVF international conference on computer vision*, 2021, pp. 22–31.
- [7] T. Huang, S. Li, X. Jia, H. Lu, and J. Liu, "Neighbor2neighbor: Self-supervised denoising from single noisy images," in *Proceedings of the IEEE/CVF conference on computer vision and pattern recognition*, 2021, pp. 14781–14790.
- [8] Y. Li, K. Zhang, J. Cao, R. Timofte, and L. Van Gool, "Localvit: Bringing locality to vision transformers," *arXiv*, 2021.
- [9] M. Sandler, A. Howard, M. Zhu, A. Zhmoginov, and L.-C. Chen, "Mobilenetv2: Inverted residuals and linear bottlenecks," in *Proceedings of the IEEE/CVF conference on computer vision and pattern recognition*, 2018, pp. 4510–4520.
- [10] K. Yuan, S. Guo, Z. Liu, A. Zhou, F. Yu, and W. Wu, "Incorporating convolution designs into visual transformers," in *Proceedings of the IEEE/CVF international conference on computer vision*, 2021, pp. 579–588.
- [11] D. Hendrycks and K. Gimpel, "Gaussian error linear units (gelus)," *arXiv*, 2016.
- [12] Z. Wang, X. Cun, J. Bao, W. Zhou, J. Liu, and H. Li, "Uformer: A general u-shaped transformer for image restoration," in *Proceedings of the IEEE/CVF conference on computer vision and pattern recognition*, 2022, pp. 17683–17693.
- [13] Y. Tang, D. Yang, W. Li, H. R. Roth, B. Landman, D. Xu, V. Nath, and A. Hatamizadeh, "Self-supervised pre-training of swin transformers for 3d medical image analysis," in *Proceedings of the IEEE/CVF conference on computer vision and pattern recognition*, 2022, pp. 20730–20740.
- [14] Z. Liu, Y. Lin, Y. Cao, H. Hu, Y. Wei, Z. Zhang, S. Lin, and B. Guo, "Swin transformer: Hierarchical vision transformer using shifted windows," in *Proceedings of the IEEE/CVF international conference on computer vision*, 2021, pp. 9992–10002.
- [15] H. Cao, Y. Wang, J. Chen, D. Jiang, X. Zhang, Q. Tian, and M. Wang, "Swin-unet: Unet-like pure transformer for medical image segmentation," in *ECCV*, 2022, pp. 205–218.
- [16] D. Jha, P. H. Smedsrud, D. Johansen, T. de Lange, H. D. Johansen, P. Halvorsen, and M. A. Riegler, "A comprehensive study on colorectal polyp segmentation with resunet++, conditional random field and test-time augmentation," *IEEE Journal of Biomedical and Health Informatics*, vol. 25, no. 6, pp. 2029–2040, 2021.
- [17] A. L. Maas, A. Y. Hannun, A. Y. Ng *et al.*, "Rectifier nonlinearities improve neural network acoustic models," in *International conference on machine learning*, vol. 30, no. 1, 2013, p. 3.
- [18] N. Kanopoulos, N. Vasanthavada, and R. L. Baker, "Design of an image edge detection filter using the sobel operator," *IEEE Journal of solid-state circuits*, vol. 23, no. 2, pp. 358–367, 1988.
- [19] D. Yu, H. Wang, P. Chen, and Z. Wei, "Mixed pooling for convolutional neural networks," in *Rough Sets and Knowledge Technology: 9th International Conference, RSKT 2014, Shanghai, China, October 24–26, 2014, Proceedings 9*, 2014, pp. 364–375.
- [20] A. Krizhevsky, I. Sutskever, and G. E. Hinton, "Imagenet classification with deep convolutional neural networks," *Advances in Neural Information Processing Systems*, vol. 25, 2012.
- [21] J. Chen, Y. Lu, Q. Yu, X. Luo, E. Adeli, Y. Wang, L. Lu, A. L. Yuille, and Y. Zhou, "Transunet: Transformers make strong encoders for medical image segmentation," *ArXiv*, 2021.
- [22] A. Hatamizadeh, Y. Tang, V. Nath, D. Yang, A. Myronenko, B. Landman, H. R. Roth, and D. Xu, "Unetr: Transformers for 3d medical image segmentation," in *Proceedings of the IEEE/CVF international conference on computer vision*, 2022, pp. 574–584.
- [23] H.-Y. Zhou, J. Guo, Y. Zhang, X. Han, L. Yu, L. Wang, and Y. Yu, "nn-former: Volumetric medical image segmentation via a 3d transformer," *IEEE Transactions on Image Processing*, 2023.
- [24] A. Kirillov, E. Mintun, N. Ravi, H. Mao, C. Rolland, L. Gustafson, T. Xiao, S. Whitehead, A. C. Berg, W.-Y. Lo *et al.*, "Segment anything," in *Proceedings of the IEEE/CVF international conference on computer vision*, 2023, pp. 4015–4026.
- [25] J. Ma, Y. He, F. Li, L. Han, C. You, and B. Wang, "Segment anything in medical images," *Nature Communications*, vol. 15, no. 1, p. 654, 2024.
- [26] Y. Xie, J. Zhang, C. Shen, and Y. Xia, "Cotr: Efficiently bridging cnn and transformer for 3d medical image segmentation," in *Medical image computing and computer-assisted intervention*, 2021, pp. 171–180.
- [27] N. Ravi, V. Gabeur, Y.-T. Hu, R. Hu, C. Ryali, T. Ma, H. Khedr, R. Rädle, C. Rolland, L. Gustafson *et al.*, "Sam 2: Segment anything in images and videos," *arXiv*, 2024.
- [28] J. Zhu, Y. Qi, and J. Wu, "Medical sam 2: Segment medical images as video via segment anything model 2," *arXiv*, 2024.
- [29] F. Milletari, N. Navab, and S.-A. Ahmadi, "V-net: Fully convolutional neural networks for volumetric medical image segmentation," in *3DV*, 2016, pp. 565–571.
- [30] J. Duchi, E. Hazan, and Y. Singer, "Adaptive subgradient methods for online learning and stochastic optimization," *Journal of machine learning research*, vol. 12, no. 7, 2011.
- [31] S. Gong, Y. Zhong, W. Ma, J. Li, Z. Wang, J. Zhang, P.-A. Heng, and Q. Dou, "3dsam-adapter: Holistic adaptation of sam from 2d to 3d for promptable medical image segmentation," *arXiv*, 2023.
- [32] W. Lei, X. Wei, X. Zhang, K. Li, and S. Zhang, "Medksam: Localize and segment anything model for 3d medical images," *arXiv*, 2023.
- [33] L. R. Dice, "Measures of the amount of ecologic association between species," *Ecology*, vol. 26, no. 3, pp. 297–302, 1945.
- [34] P. Bilic, P. Christ, H. B. Li, E. Vorontsov, A. Ben-Cohen, G. Kaissis, A. Szeskin, C. Jacobs, G. E. H. Mamani, G. Chartrand *et al.*, "The liver tumor segmentation benchmark (lits)," *Medical Image Analysis*, vol. 84, p. 102680, 2023.
- [35] *Proceedings of the Third International Symposium on Image Computing and Digital Medicine, ISICDM 2019, Xi'an, China, August 24–26, 2019*, 2019.
- [36] B. Landman, Z. Xu, J. Igelsias, M. Styner, T. Langerak, and A. Klein, "Medical image computing and computer-assisted intervention multi-atlas labeling beyond the cranial vault—workshop and challenge," in *Medical image computing and computer-assisted intervention*, vol. 5, 2015, p. 12.